











## BRIEF COMMUNICATION

# Longitudinal advanced MRI case report of white matter radiation necrosis

Vanessa Wiggermann<sup>1,2,3,\*</sup> , Emmanuelle Lapointe<sup>4,\*</sup> , Ludmila Litvin<sup>5</sup> , Carina Graf<sup>1,6</sup> , Eneidino Hernández-Torres<sup>2,3</sup> , Michael McKenzie<sup>7</sup>, Irene M. Vavasour<sup>3,5</sup>, Cornelia Laule<sup>1,5,6,8</sup> , Erin L. MacMillan<sup>3,5,9</sup> , David K. B. Li<sup>4,5</sup> , Shannon H. Kolind<sup>1,4,5</sup>, Alexander Rauscher<sup>1,2,3,5</sup>  & Anthony L. Traboulsee<sup>4</sup> 

<sup>1</sup>Department of Physics and Astronomy, University of British Columbia, Vancouver, British Columbia, Canada

<sup>2</sup>Department of Pediatrics, University of British Columbia, Vancouver, British Columbia, Canada

<sup>3</sup>UBC MRI Research Centre, University of British Columbia, Vancouver, British Columbia, Canada

<sup>4</sup>Department of Medicine, Division of Neurology, University of British Columbia, Vancouver, British Columbia, Canada

<sup>5</sup>Department of Radiology, University of British Columbia, Vancouver, British Columbia, Canada

<sup>6</sup>International Collaboration on Repair Discoveries (ICORD), University of British Columbia, Vancouver, British Columbia, Canada

<sup>7</sup>Department of Surgery, Division of Radiation Oncology and Developmental Radiotherapeutics, University of British Columbia, Vancouver, British Columbia, Canada

<sup>8</sup>Department of Pathology & Laboratory Medicine, University of British Columbia, Vancouver, British Columbia, Canada

<sup>9</sup>Philips, Markham, Ontario, Canada

## Correspondence

Vanessa Wiggermann, UBC MRI Research Centre, University of British Columbia, M10 Purdy Pavilion, 2221 Wesbrook Mall, Vancouver, BC V6T 2B5, Canada. Tel: 604-822-7241; Fax: 604-827-3339; E-mail: vwiggerm@phas.ubc.ca

## Funding Information

This study was in part supported by the German Academic Exchange Service (DAAD).

Received: 15 August 2018; Revised: 9 October 2018; Accepted: 31 October 2018

*Annals of Clinical and Translational Neurology* 2019; 6(2): 379–385

doi: 10.1002/acn3.704

\*These authors contributed equally to the manuscript.

This work has been presented in an abstract form (poster presentation) at the 69th Annual American Academy of Neurology meeting in Boston, April 2017.

## Introduction

Arteriovenous malformations (AVMs) are infrequent but can lead to severe neurological deficits if bleeding occurs. Symptomatic and ruptured AVMs, at high risk for rebleeding, are often surgically resected. Alternatively, stereotactic radiosurgery (SRS) may be used if AVMs are nonamenable to surgery, for instance if located in

## Abstract

Radiation necrosis mostly occurs in and near the radiation field. We used magnetic resonance imaging to study radiation-induced necrosis of atypical onset, severity, and extent following stereotactic radiosurgery for a symptomatic arteriovenous malformation. Susceptibility-sensitive imaging, T<sub>1</sub>-relaxation, myelin water imaging, and magnetic resonance spectroscopy were acquired three times up to 52 months postradiosurgery. Increasing water content outside the radiation field, contralateral neuronal loss, and gliosis were detected over time. Our findings suggest that radiation-induced vasculopathic changes spread more diffusely than previously described. An autoimmune response to brain antigens could underlie white matter changes outside the initial radiation field.

eloquent brain areas. However, SRS carries an up to 19% risk of delayed radiation necrosis (RN).<sup>1</sup> The mechanisms underlying RN are not fully understood, but animal models suggest that endothelial cell damage leads to vasculopathic changes, increased blood–brain barrier permeability and vasogenic edema.<sup>2</sup> Oligodendrocyte damage with subsequent demyelination has also been implicated.<sup>2</sup> RN typically occurs at least 3 months, but often much

later, post-SRS and affects tissue within the radiation field. The risk is linked to the cumulative radiation dose and volume of tissue receiving 12-Gy.<sup>1,3,4</sup> Age has also been suggested as a risk factor, with potentially increased likelihood and earlier onset RN observed in pediatric patients.<sup>5</sup>

Conventional magnetic resonance imaging (MRI) displays T<sub>2</sub>-hyperintensity and T<sub>1</sub>-contrast-enhancement in the radiation field and can support RN diagnosis.<sup>3</sup> Nevertheless, these findings are unspecific and may therefore impede RN diagnosis and early intervention in atypical cases. Quantitative MRI can provide clarification of the pathophysiological processes<sup>3</sup> related to RN. Previous studies focused on proton MR spectroscopy (MRS), perfusion and diffusion imaging. The existing MRS literature suggests that reduced N-acetyl-aspartate (NAA), total creatine (tCr), and choline (Cho) could help identify RN also in atypical cases.<sup>6</sup>

Here, we collected quantitative MRI data longitudinally to study a young female with suspected RN post-SRS from AVM treatment, who presented with white matter (WM) injury of uncharacteristic early onset, atypical severity, and extent.<sup>1,3</sup> We focused on susceptibility-sensitive imaging (SSI) for monitoring of the AVM nidus and T<sub>1</sub>-relaxation as a surrogate measure for changes in water content in the surrounding tissue; myelin water imaging to detect demyelination as a reflection of oligodendrocyte or tissue damage; and MRS to describe metabolic changes, which we compared to existing literature.

## Methods

The study was approved by the local ethics committee and patient consent was obtained. The 17-year-old female had a ruptured 5.6 cm<sup>3</sup> Spetzler-Martin grade II left motor cortical AVM (Fig. 1A) causing migratory right-sided sensory symptoms. As the AVM was located in an eloquent brain area, it was treated with linear accelerator-based SRS in a single-fraction 80% isodose of 20-Gy (Fig. 1B), encompassing a 12-Gy volume of 27.97 mL. As soon as 2 months post-SRS, the patient presented with worsening right hemiparesis, expressive dysphasia, and focal hand motor seizures. Atypical MRI findings were noted on eight conventional MRIs performed at months 3, 9, 16, 21, 37, 40, 43, and 51 post-SRS as part of the clinical follow-up. Three months following SRS, conventional MRIs were suggestive of RN, showing hyperintense T<sub>2</sub>-signal and patchy enhancement in the radiation field (Fig. 1E and I). Clinical symptoms and radiological features subsequently worsened despite conservative treatment for RN consisting of a total of five courses of high-dose steroids over 18 months. Advanced MRI, including SSI, quantitative T<sub>1</sub>-relaxation (qT<sub>1</sub>) and quantitative T<sub>2</sub>-relaxation data were acquired at three time points,

months 22, 43, and 52 post-SRS, to characterize the ongoing tissue damage. MRS data were also collected, at months 22 and 52 only. All MRI data were acquired on a Philips 3T Achieva using either a transmit/receive (MRS) or eight-channel SENSE head coil.

At both time points, MRS data were acquired near the AVM and in the right centrum semiovale (CSO) as shown in Figure 2 (top). MRS data were analyzed with LC Model,<sup>7</sup> including frequency alignment and eddy current correction. Metabolite concentrations were corrected for WM-gray matter compartmentation and T<sub>1</sub>/T<sub>2</sub> relaxation using FSL's FAST<sup>8</sup> and literature relaxation values.<sup>9</sup> All metabolites were compared to an age, sex and ethnicity-matched control.

Myelin water fraction (MWF) maps were estimated from quantitative T<sub>2</sub>-relaxation data using voxel-wise multiexponential fitting, including spatial regularization and correction for stimulated echoes.<sup>10</sup> qT<sub>1</sub>, venograms from susceptibility-weighted images (SWI) and R<sub>2</sub>\* maps were computed as described previously.<sup>11–13</sup> Images were coregistered using FSL's FLIRT and five regions of interest were evaluated: the anterior left frontal WM, which appeared initially healthy; the genu of the corpus callosum; the anterior and posterior right frontal WM, and the right CSO T<sub>2</sub>-hyperintensities.

## Results

### Laboratory findings

Investigation for systemic vasculitis and infections was negative. A lumbar puncture at month 20 showed normal IgG index, leukocyte and protein count, and no oligoclonal band. At month 58, surgical resection of the AVM following rebleeding showed necrosis consistent with RN in the adjacent brain tissue.

### Conventional MRI findings

Nine months post-SRS, six new FLAIR-abnormalities with restricted diffusion appeared remote from and contralateral to the radiation field including three brainstem abnormalities of which one was located in the right posterior midbrain (Fig. 1C) and three in the right CSO (Fig. 1D). Thereafter, in addition to the presence of enlarging cystic cavities at the main radiation site, the FLAIR-hyperintensity expanded to involve the majority of the left hemisphere (Fig. 1E–H). Contrast enhancement persisted within the AVM (Fig. 1I–L). Hyperbaric oxygen therapy (HBOT) treatment prior to month 51 resulted in a mild reduction of the FLAIR-hyperintense area without clinical change in the patient.

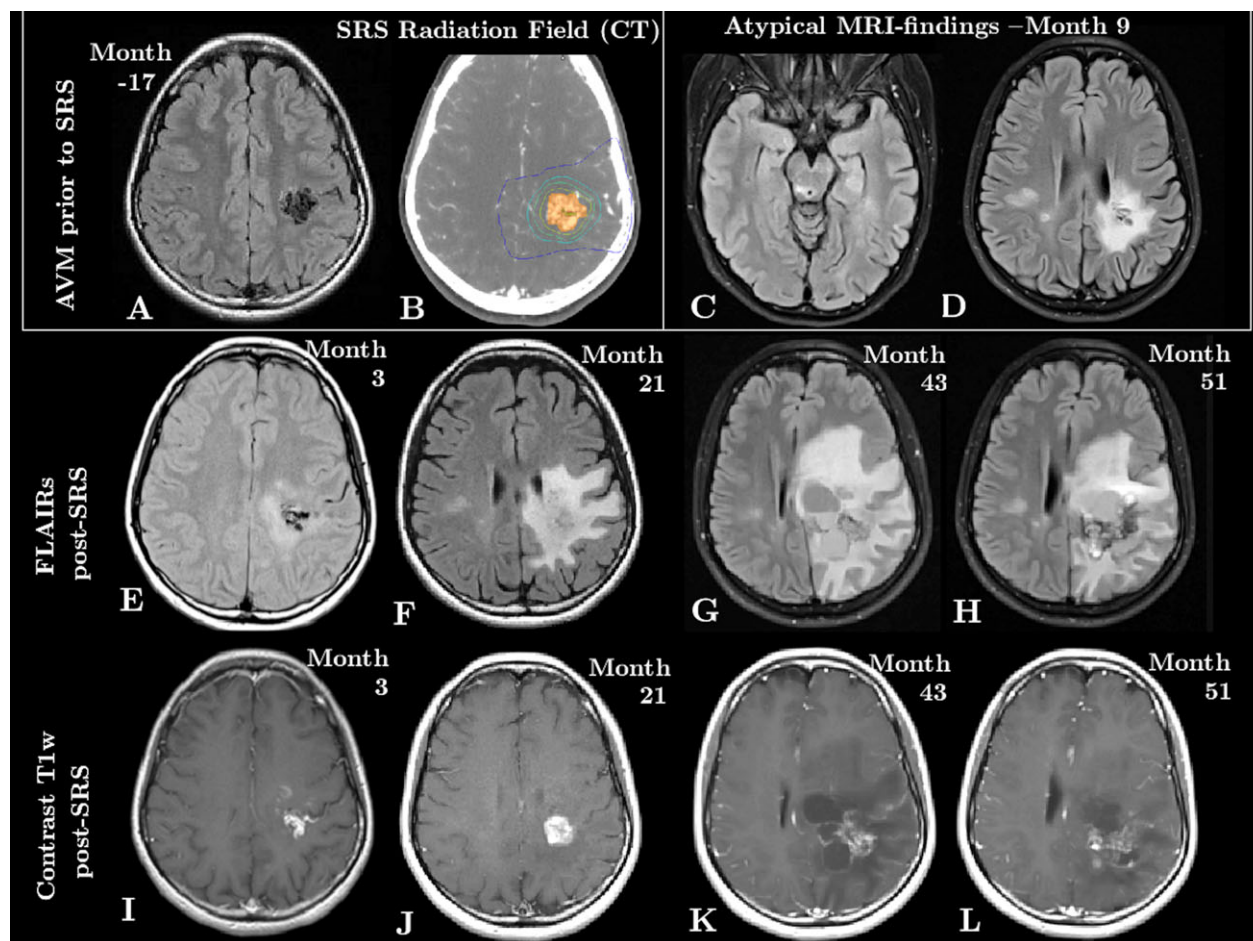


**Figure 1.** Clinical MRI changes over time. A and B show the AVM prior to treatment, on FLAIR (A) and on CT (B), which was used for treatment planning. C and D capture the atypical MRI findings apparent at month 9: FLAIR hyperintensities remote from the AVM in the posterior midbrain (C) and in the right centrum semiovale (D). The bottom two rows show the evolution of the AVM post-SRS, demonstrating an expansion of the area of damage on FLAIR (E-H) and persistent enhancement of the AVM on postcontrast T<sub>1</sub>w images (I-L).

Quantitative results for all regions-of-interest are summarized in Tables S1 and S2.

### MRS adjacent to the left motor cortex AVM (yellow voxel)

At month 22, decreases in glutamate (Glu), tCr, and NAA were observed in the vicinity of the radiation field (Fig. 2, center) as well as the presence of lactate, all in keeping with neuronal loss.<sup>14</sup> Glutamine (Gln) was increased by five times the control's value, while myoinositol (mI) was reduced.

### MRS in the right CSO (blue voxel)

N-acetyl-aspartate was also decreased in the right CSO voxel overlying the FLAIR-hyperintensities at both time points, although less than adjacent to the AVM. At

month 22 and to a lesser extent at month 52 (Fig. 2, bottom), mI and Cho (not shown) were present in concentrations exceeding control values. Gln was also increased but found in lower concentrations than near the AVM. The month 52 spectrum near the AVM was excluded from analysis due to the presence of blood products.

### Susceptibility-weighted-venograms

Minimum intensity projections of the susceptibility-weighted venograms computed at each time point, display the thrombus in the AVM and its increasing involvement of the venous network (Fig. 3A).

### Quantitative MRI changes

The qT<sub>1</sub> increase in the left anterior frontal WM from month 22 to 44 (Fig. 3B), in parallel with the development

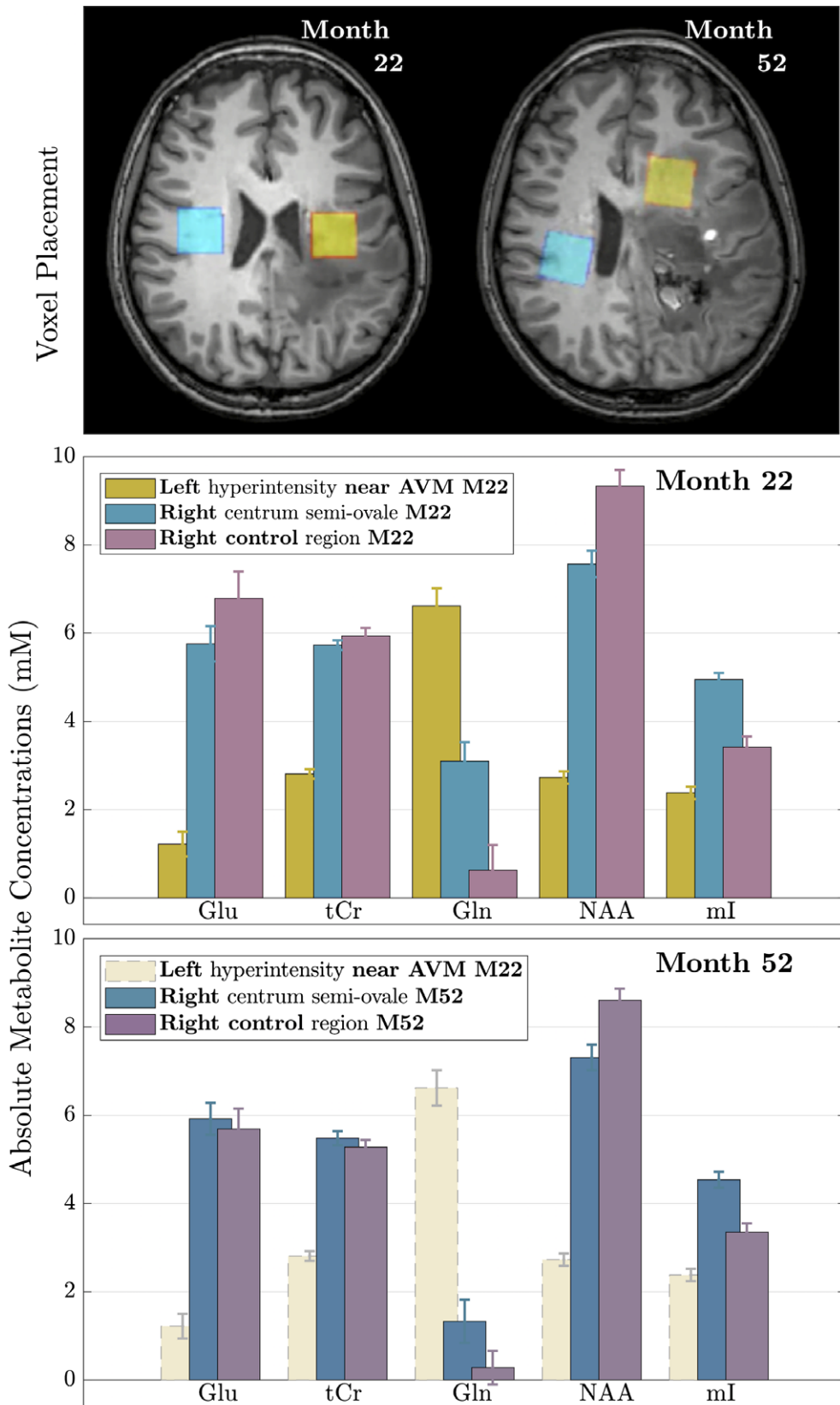


**Figure 2.** MRS result overview. On the top, the spectroscopy voxel placement at months 22 and 52 is shown. Absolute metabolite concentration measurements  $\pm$  SD near the AVM (yellow) and in the right CSO (blue/green) compared to an age-matched healthy control (purple) are shown at month 22 (middle) and month 52 (bottom). Note that the left voxel (yellow, near the AVM) at month 52 could not be evaluated due to the presence of blood products and the month 22 data is shown for comparison. (Glu: Glutamate; tCr: total Creatine; Gln: Glutamine; NAA: N-acetyl-aspartate; ml: myoinositol).

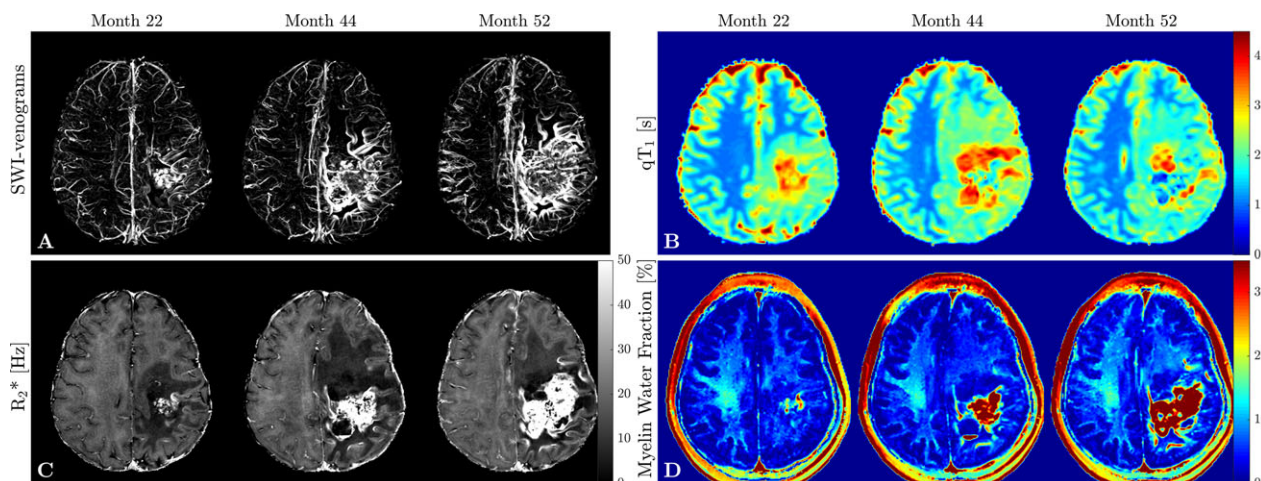


**Figure 3.** Summary of quantitative MRI findings. (A) Minimum intensity projections of SWI-Venograms demonstrate an increasing venous involvement and thrombus in the AVM; (B)  $qT_1$  maps representative of changes in water content show an increase in  $qT_1$  in line with the presence of edema at month 44 and recovery at month 52 in the anterior frontal WM region of interest; (C)  $R_2^*$  decreased in the left anterior frontal WM at first and recovered at month 52. Note also the clear depiction of the overall involvement of the left hemisphere; (D) In line with the observed  $qT_1$  and  $R_2^*$  changes, MWF maps show an initial decrease in the left anterior frontal WM at month 44 and subsequent partial recovery likely due to resolution of edema.

of FLAIR-hyperintensity in this initially normal-appearing area, likely reflects spreading of vasogenic edema. The subsequent, less pronounced,  $qT_1$  decrease following HBOT suggests partial resolution of edema.  $R_2^*$  (Fig. 3C) and MWF (Fig. 3D) likewise decreased initially due to increased presence of water<sup>15</sup> and recovered subsequently. The right anterior frontal WM also demonstrated mild increases in  $qT_1$  between months 22–52. None of the other regions exhibited changes over time. Notably, there was no ongoing myelin loss in the right CSO lesions.

## Discussion

The combined observation of neuronal loss and gliosis supports extensive RN as the underlying process, given the overall clinical context and consistent MRS literature findings. The metabolic changes observed contralateral to the SRS-field suggest radiation-induced vasculopathic changes that are reflected in the appearance of the right CSO and brain stem  $T_2$ -hyperintensities 9 months post-SRS. Wallerian degeneration through the corpus callosum could have caused contralateral tissue damage, but would not anatomically explain a right posterior midbrain lesion.<sup>16</sup>

The bilateral Gln elevation could have resulted from hypoxia or gliosis<sup>14,17</sup> occurring with RN, the latter more

likely given that Glu was bilaterally decreased, not increased as expected with hypoxia, and ml, another glial marker,<sup>14</sup> was also increased in the right CSO. The decrease in Gln from months 22 to 52, despite stability of the right CSO  $T_2$ -hyperintensities, indicates potential reversibility of tissue injury rather than irreversible Wallerian degeneration. Whether HBOT contributed to the decrease in Gln remains uncertain, and although its timing coincided with the observed reduction of RN-related vasogenic edema, there was no associated clinical improvement.

While tissue edema linked to radiation-induced injury can be impressive, RN classically does not exceed the radiation field. As highlighted, the patient was at increased risk for RN given her young age and the 12 Gy-receiving volume,<sup>3,4</sup> possibly favoring the development of extensive and severe tissue injury. Foci of RN contralateral to the radiation field are relatively rare.<sup>18,19</sup> In some cases, biopsies showed gliosis and necrosis consistent with RN but also plasma cell infiltrate and transmural vessel T-cell infiltration consistent with vasculitis suggesting immune system involvement.<sup>18,19</sup> In the present case, the tissue biopsy did not provide much information about the remote injuries. Despite the lack of indirect evidence of immunogenicity in the cerebrospinal fluid (no oligoclonal band or elevated

IgG index), it remains possible that an autoimmune response to brain antigens released in the necrotic area may be responsible for the distant damage.<sup>20</sup>

## Conclusion

Advanced MRI can be useful to confirm RN in atypical cases, with MRS suggesting that radiation-induced vasculopathic changes develop outside of and contralateral to the SRS-field. These changes appear to be based on gliosis and neuronal loss, rather than demyelination. Our data indicate that RN occurs more diffusely than previously described.

## Acknowledgment

The authors would like to acknowledge Dr. Ian MacKenzie, pathologist at Vancouver General Hospital, University of British Columbia, for interpreting and providing pathology findings of the resected brain tissue. VW and CG are supported by graduate studentship awards from the MS Society of Canada. SHK is grateful for support from the MS Society of Canada and the Milan & Maureen Ilich Foundation. AR acknowledges support from NSERC, Canada Research Chairs, and the National MS Society.

## Conflict of Interest

Vanessa Wiggermann has nothing to disclose. Emmanuelle Lapointe has received consulting fees from Roche, Biogen, and EMD Serono and speaker fees from Genzyme and EMD Serono. Ludmila Litvin, Carina Graf, and Eneidino Hernández-Torres report no disclosures. Michael McKenzie is on the Steering Committee for a randomized trial in prostate cancer sponsored by Janssen R&D. He has received honoraria from Abbott, Bayer, Amgen, and Ferring as well as from Varian. Irene M Vavasour and Cornelia Laule have no disclosures. Erin L. Macmillan is supported by Philips Healthcare Canada. David Li has received research funding from the Canadian Institute of Health Research and Multiple Sclerosis Society of Canada. He is the Emeritus Director of the UBC MS/MRI Research Group, which has been contracted to perform central analysis of MRI scans for therapeutic trials with Novartis, Perceptives, Roche, and Sanofi-Aventis. The UBC MS/MRI Research Group has also received grant support for investigator-initiated independent studies from Genzyme, Merck-Serono, Novartis, and Roche. He has acted as a consultant to Vertex Pharmaceuticals and served on the Data and Safety Advisory Board for Opexa Therapeutics and Scientific Advisory Boards for Adelphi Group, Celgene, Novartis, and Roche. He has also given lectures which have been

supported by nonrestricted education grants from Biogen-Idec, Novartis, Sanofi-Genzyme, and Teva. Shannon Kolind has consulted for Acorda and Genzyme. She has received research support from Roche. She is grateful for support from the MS Society of Canada and the Milan & Maureen Ilich Foundation. Alexander Rauscher has received funding from NSERC and the National MS Society as well as speaker fees from Philips Medical. Anthony Traboulsee has received grant funding from the MS Society of Canada, Canadian Institute for Health Research, Roche, and Genzyme; he also received honoraria or travel grants from Teva Canada Innovation, Roche, Merck/EMD Serono, Genzyme, Chugai Pharmaceuticals.

## Author Contribution

As advanced MRI findings are central to this case report, experts in every MR modality as well as clinicians involved in the case management have been included as authors in this manuscript. Details on the role of every author are provided below:

Vanessa Wiggermann: Data acquisition design, analysis, and interpretation of data, drafting, and revising the manuscript for content.

Emmanuelle Lapointe: Interpretation of data, drafting, and revising the manuscript for content.

Ludmila Litvin: Analysis and interpretation of data, revising the manuscript for content.

Carina Graf: Analysis and interpretation of data, revising the manuscript for content.

Eneidino Hernández-Torres: Analysis and interpretation of data, revising the manuscript for content.

Michael McKenzie: Drafting/revising the manuscript for content.

Irene M. Vavasour: Study coordination, interpretation of data, revising the manuscript for content.

Cornelia Laule: Interpretation of data, revising the manuscript for content.

Erin L. MacMillan: Data acquisition design, interpretation of data, revising the manuscript for content.

David K.B. Li: Interpretation of data, revising the manuscript for content.

Shannon H. Kolind: Study concept and design, interpretation of data, revising the manuscript for content.

Alexander Rauscher: Interpretation of data, revising the manuscript for content.

Anthony L. Traboulsee: Interpretation of data, revising the manuscript for content.

## References

1. Herbert C, Moissenko V, McKenzie M, et al. Factors predictive of symptomatic radiation injury after linear

- accelerator-based stereotactic radiosurgery for intracerebral arteriovenous malformations. *Int J Radiat Oncol Biol Phys* 2012;83:872–877.
2. Rahmathulla G, Weil RJ. Cerebral radiation necrosis: a review of the pathobiology, diagnosis and management considerations. *J Clin Neurosci* 2013;20:485–502.
  3. Chao ST, Ahluwalia MS, Barnett GH, et al. Challenges with the diagnosis and treatment of cerebral radiation necrosis. *Int J Radiat Oncol Biol Phys* 2013;87:449–457.
  4. Kano H, Flickinger JC, Tonetti D, et al. Estimating the risks of adverse radiation effects after gamma knife radiosurgery for arteriovenous malformations. *Stroke* 2017;48:84–90.
  5. Plimpton SR, Stence N, Hemenway M, et al. Cerebral radiation necrosis in pediatric patients. *Pediatr Hematol Oncol* 2015;32:78–83.
  6. Sundgren PC. MR spectroscopy in radiation injury. *AJNR* 2009;30:1469–1476.
  7. Provencher SW. Estimation of metabolite concentrations from localized in vivo proton NMR spectra. *Magn Reson Med* 1993;30:672–679.
  8. Zhang Y, Brady M, Smith S. Segmentation of brain MR images through a hidden Markov random field model and the expectation-maximization algorithm. *IEEE Trans Med Imag* 2001;20:45–57.
  9. Vavasour IM, Laule C, Kolind SH, et al. Hydration status does not affect brain water content or myelin water fraction in healthy volunteers. *Proc Intl Soc Mag Reson Med* 2009;17:3217. Honolulu, Hawaii.
  10. Prasloski T, Mädler B, Xiang Q-S, et al. Applications of stimulated echo correction to multicomponent T2 analysis. *Magn Reson Med* 2012;67:1803–1814.
  11. Deoni SCL. High-resolution T1 mapping of the brain at 3T with driven equilibrium single pulse observation of T1 with high-speed incorporation of RF field inhomogeneities. *J Magn Reson Imaging* 2007;26:1106–1111.
  12. Denk C, Rauscher A. Susceptibility weighted imaging with multiple echoes. *J Magn Reson Imaging* 2010;31:185–191.
  13. Fernández-Seara MA, Wehrli F. Postprocessing technique to correct for background gradients in image-based R2\* measurements. *Magn Reson Med* 2000;44:358–366.
  14. Govindaraju V, Young K, Maudsley AA. Proton NMR chemical shifts and coupling constants for brain metabolites. *NMR Biomed* 2000;13:129–153.
  15. Brant-Zawadzki M, Bartkowski H, Ortendahl DA, et al. NMR in experimental cerebral edema: value of T1 and T2 calculations. *AJNR* 1984;5:125–129.
  16. Benarroch EE, Daube JR, Flemming KD, Westmoreland BF. *Mayo clinic medical neurosciences: organized by neurologic systems and levels*, 5th edition by Informa Healthcare. New York: Oxford University Press; 2008. 824 pages.
  17. Oz G, Tkáč I, Charnas LR, et al. Assessment of adrenoleukodystrophy lesions by high field MRS in non-sedated pediatric patients. *Neurology* 2005;8:434–441.
  18. Xu LW, Recht L. Nimg-74 enhancing lesions outside the irradiated field in anaplastic oligodendroglioma: tumor or not? *Neuro-Oncol* 2015;17(suppl 5):v171.
  19. Rauch PJ, Park HS, Knisely JPS, et al. Delayed radiation-induced leukoencephalopathy. *Int J Radiat Oncol Biol Phys* 2012;83:369–375.
  20. Lumniczky K, Szatmári T, Sáfrány G. Ionizing radiation-induced immune and inflammatory reactions in the brain. *Front Immunol* 2017;8:517.

## Supporting Information

Additional supporting information may be found online in the Supporting Information section at the end of the article.

**Table S1.** Summary of the three quantitative MR metrics ( $qT_1$ ,  $R_2^*$ , MWF), compared over time. Arrows indicate the direction of change that occurred with respect to the previous time point. Asterisks indicate changes between months 22 and 52. Values are highlighted in bold font as different from other time points, if the mean values are separated by at least one standard deviation. (AF: anterior-frontal; WM: white matter; PF: posterior-frontal; CSO: centrum semiovale; SD: standard deviation).

**Table S2.** Summary of the MRS changes over time and compared to healthy control data. Asterisks indicate changes between months 22 and 52. (+) or (-) indicate negative or positive differences with respect to the control values for all metabolites, shown in blue in the middle column, at the same time points. Values are highlighted in bold font as different from control values at each time point, and between time points, if the respective mean values are separated by at least one standard deviation. (Les: Lesions; CSO: centrum semiovale; Glu: Glutamate; tCr: total Creatine; Gln: Glutamine; NAA: N-acetyl-aspartate; mI: myoinositol; tCho: total Choline; HC: healthy control).